SR OPTICAL CLOCK WITH HIGH STABILITY AND ACCURACY*

A. LUDLOW, S. BLATT, M. BOYD, G. CAMPBELL, S. FOREMAN, M. MARTIN, M. H. G. DE MIRANDA, T. ZELEVINSKY, AND J. YE

JILA, National Institute of Standards and Technology and University of Colorado
Boulder, Colorado 80309-0440, USA
E-mail: Ye@JILA.colorado.edu

T. M. FORTIER, J. E. STALNAKER, S. A. DIDDAMS, C. W. OATES, Z. W. BARBER, AND N. POLI†

National Institute of Standards and Technology
325 Broadway, Boulder, Colorado 80305, USA

We report on our recent evaluations of stability and accuracy of the JILA Sr optical lattice clock. We discuss precision tools for the lattice clock, including a stabilized clock laser with sub-Hz linewidth, fs-comb based technology allowing accurate clock comparison in both the microwave and optical domains, and clock transfer over optical fiber in an urban environment. High resolution spectroscopy ($Q > 2 \times 10^{14}$) of lattice-confined, spin-polarized strontium atoms is used for both a high-performance optical clock and atomic structure measurement. Using a Ca optical standard for comparison, the overall systematic uncertainty of the Sr clock is reduced to $< 2 \times 10^{-16}$.

1. Introduction

Optical atomic clocks derive their advantages in stability and accuracy from the enhanced measurement precision arising from large line quality factors (Q) that now exceed 10^{14} [1, 2]. The lattice clock technique [1, 3-7] presents an intriguing situation in which one benefits from a large signal-to-noise ratio (S/N) provided by a neutral atom ensemble, while enjoying many of the spectroscopic features of single trapped ions. The lattice potential provides Lamb-Dicke confinement where the resonance feature of interest is not influenced by atomic motion, enabling high precision, high accuracy measurements.

The weakly allowed $^1S_0$ - $^3P_0$ transition in alkaline-earth(-like) atoms is particularly well suited for such a scheme due to the existence of a magic wavelength where the ac Stark shift from the trapping laser is identical for the two clock states, and the insensitivity of the states to lattice polarization. The accuracy of a lattice clock based on ^{87}Sr is expected to reach below 10^{-17}, while

*This work is supported by NIST, ONR, and NSF.

†also with Dipartimento di Fisica and LENS, Università di Firenze, INFN-Sezione di Firenze, Via N. Carrara 1 I-50019 Sesto Fiorentino (FI), Italy

the stability could reach below 10^{-16} at 1 s when probed by a sufficiently stable optical local oscillator. Such accuracy and precision goals will require focused efforts in both laser development and precision spectroscopy. In this paper we report the present status of our clock system, including local oscillator performance, clock comparison technology using fs-combs, high resolution spectroscopy, and the current level of accuracy and stability of the lattice clock.

2. OPTICAL CLOCKWORK

2.1. *Stable Optical Local Oscillator*

For the purposes of operating an optical clock with the best possible stability, it is necessary for the probe laser to have an exceedingly long phase-coherence time. Development of such an oscillator to probe the Sr clock transition at 698 nm has therefore been one of the central focuses of our work. The stabilization scheme for our laser is discussed in detail elsewhere [8]. Briefly, a grating-stabilized diode laser is locked to a high-finesse ultra-low-expansion (ULE) cavity mounted in a vertical orientation to reduce fluctuations of the cavity length due to vibrations [9]. The cavity is under vacuum and mounted on a compact, passive vibration-isolation table.

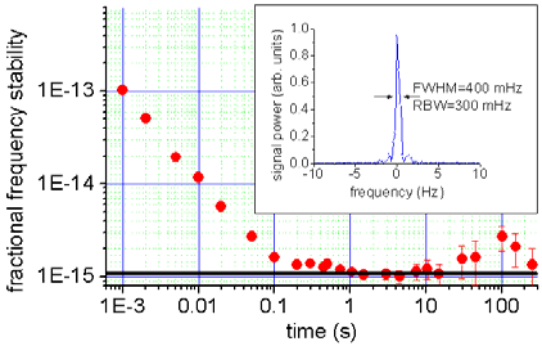

Figure 1. Allan deviation (with a linear drift removed) for a heterodyne beat between two independent clock laser systems at 698 nm. The ~1 × 10^{-15} stability at 0.1 – 1000 s is consistent with the estimated thermal noise limit. The inset shows the beat between the lasers is well below 1 Hz for an integration time of a few seconds.

The clock laser performance has been characterized in a number of ways, including direct comparison of two similar systems at 698 nm, comparison to highly stabilized lasers at other colors using the fs-comb, and by precision atomic spectroscopy. Direct comparison between the two 698 nm systems via heterodyne beat reveals narrow linewidths often below 300 mHz for integration times of a few seconds (see the inset of Fig. 1). The Allan deviation shown in

Fig. 1 reveals that the fractional frequency noise of the beat is ~1 × 10^{-15} at 0.1 – 1000 s, consistent with the expected limit set by thermal-mechanical noise in the cavity mirrors and mirror coatings [10].

2.2. *Optical Frequency Comb Clockwork and Precision Fiber Transfer*

The femtosecond optical comb plays an essential role for clock development. It provides a coherent link between high accuracy clocks operating in either the optical or microwave domains. For absolute frequency measurements, a direct-octave-spanning, self-referenced frequency comb similar to that reported in [11] is stabilized by the clock laser at 698 nm. The comb provides a measurement of the laser frequency relative to a microwave signal derived from a hydrogen maser calibrated to the NIST primary Cs fountain clock [12]. To enable the microwave comparison, a diode laser operating near 1320 nm is amplitude-modulated and transmitted over a 3.5-km fiber optic link from NIST to JILA [13, 14]. The instability of the frequency-counting signal is ~2.5 × 10^{-13} for a 1-s integration time. The periodic stretching and compressing of the fiber, associated with daily temperature cycles, has been found to cause frequency offsets as large as 10^{-14}. Stabilization of the fiber link is thus implemented for high accuracy clock comparisons [14].

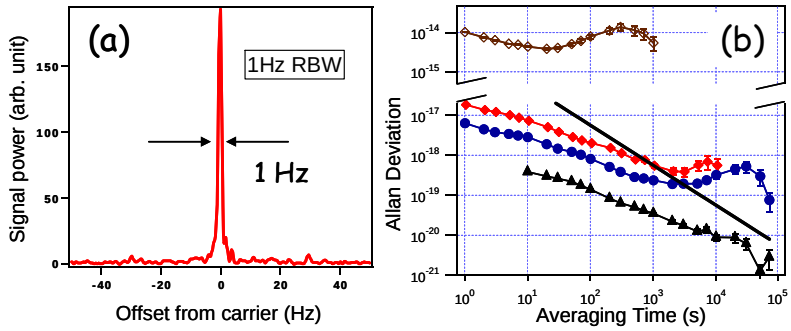

Figure 2. (a) Optical beat between the fiber-transferred laser and the NIST comb at 1064 nm. The fs-comb in JILA is stabilized to the 698 nm clock laser, distributing the stability across the optical spectrum. A JILA 1064 nm Nd:YAG laser is stabilized to the comb and used as a transfer laser to NIST over a 3.5 km fiber which is optical-phase stabilized. At NIST, a second fs-comb stabilized to the 1123 nm Hg^{+} clock laser is used to compare the two stable oscillators. The beat linewidth between the NIST comb and the transfer laser is 1 Hz. (b) Instability of the transfer systems. Open diamonds are typical passive instabilities of the 7- and 32-km fiber links. Closed diamonds (circles) are for the 32-km (7-km) fiber transfer system. Black triangles represent in-loop performance. The solid line represents 1 radian of accumulated phase noise during the averaging time.

The comb and fiber link also support transmission of stable optical frequencies between JILA and NIST. First, the comb is used to distribute the Sr clock stability across the optical spectrum, allowing use of a transfer laser at

1064 nm. We have examined the precision of the distribution across the comb spectrum by comparing our 698 nm clock laser with a similar independent system operating at 1064 nm [9]. The resulting beat between the stabilized comb and the 1064 nm laser has a linewidth below 0.5 Hz, verifying the ability of the comb to fully preserve the optical phase coherence. For transfer of the clock signal, a 1064 nm laser is phase-locked to the comb and sent through the fiber to the NIST laboratory where it is measured relative to a number of high accuracy optical clocks [15, 16, 7] using a second fs-comb [17]. To eliminate noise induced by the transfer, the 1064 nm light is partially reflected back to our lab allowing interferometric stabilization of the link [18]. Figure 2 (a) shows a beat between the transfer laser and a NIST fs-comb that is stabilized to a local oscillator used for the Hg^{+} clock [19]. The beat has a resolution-bandwidth-limited linewidth of 1 Hz, demonstrating that the phase coherence of the two clock lasers is not degraded by the two fs-combs and the fiber transfer process. In addition, Fig. 2(b) summarizes results of passive and phase-stabilized optical transfer for 7 km (the round trip length of our fiber link) and 32 km fiber lengths. The transfer noise of the stabilized fiber links is $\sim 1 \times 10^{-17}$ at 1 s [18].

3. High resolution Spectroscopy

Lattice-confined fermionic ^{87}Sr atoms are used for an accurate atomic reference. ^{87}Sr atoms are laser cooled in two stages [20, 4], first via a broad (32 MHz) and then a narrow (7.4 kHz) cycling transition. A vertical one-dimensional optical lattice is overlapped with the atomic cloud as the atoms are cooled in the second stage magneto-optic trap. After the cooling cycle is finished, roughly 10^4 atoms remain trapped in the lattice, at a temperature of ~2 μK.

3.1. *Spectroscopy in the Magic Wavelength Lattice*

The lattice potential is sufficiently deep such that the $^1S_0$ - $^3P_0$ clock transition is probed in the Lamb-Dicke regime along the lattice axis where the spatial dimension of the confinement is small compared to the interrogation wavelength. The resulting absorption spectrum is free of Doppler or recoil effects, allowing high line Q's to be achieved. When the transition is strongly saturated, spectra such as that in Fig. 3 (a) are observed. Here the narrow transition is accompanied by motional sidebands. The sideband spectrum is useful for direct measurement of the thermal-mechanical properties of the trapped atoms, including temperatures and trap motional frequencies [4]. The narrow central feature serves as the atomic reference as it excludes any motional or Stark broadenings when the magic wavelength lattice is used. In the unsaturated case, this carrier transition has a width of ~5 Hz, shown in Fig. 3(b), representing a line Q of 10^{14}.

3.2. *Nuclear Spin Effects*

The limit to the achievable line Q in Fig. 3(b) is mainly due to the magnetic sensitivity of the clock transition. The hyperfine state mixing, which leads to the ~1 mHz linewidth of the otherwise forbidden clock transition, increases the magnetic moment of the $^3P_0$ state, resulting in a small differential *g*-factor between $^3P_0$ and $^1S_0$. The resultant sensitivity of the clock transition to magnetic fields requires careful clock design to ensure frequency stability and accuracy.

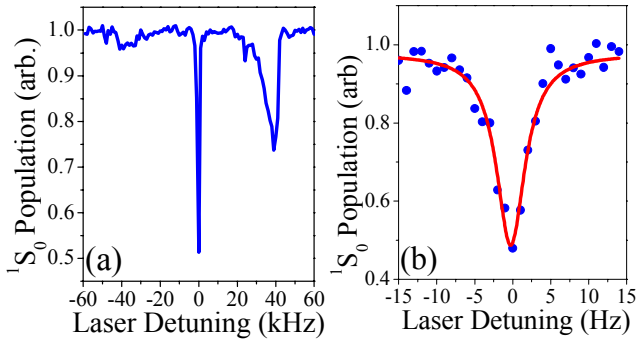

Figure 3. High resolution spectroscopy of lattice confined ^{87}Sr atoms. (a) Resolved longitudinal sideband spectrum observed when the transition is strongly saturated. The trap frequency is determined from the carrier-sideband separation. The atom temperature can be extracted from the lineshape of the sidebands, which are asymmetrically broadened due to motion in the trap. (b) The narrow carrier transition used as the atomic reference. Here the 5 Hz linewidth is limited by residual magnetic fields.

To determine the magnitude of the differential *g*-factor, we have performed NMR-like measurements on various m_F-sublevels of the clock transition in the presence of a bias magnetic field. Figure 4(a) shows the absorption spectrum in the presence of a bias field using linearly polarized light to drive ten possible π-transitions ($\Delta m_F = 0$). In Fig. 4(b), the probe light polarization is rotated by 90° from the quantization axis such that nine σ^- ($\Delta m_F = -1$) and nine σ^+ ($\Delta m_F = +1$) transitions are observed simultaneously. While the π-transitions would be sufficient for measurement of the differential *g*-factor magnitude, the $\sigma^{+/-}$ transitions provide more information as the spectrum depends on both the magnitude and the sign of the effect (i.e. the state mixing *increases* the $^3P_0$ *g*-factor). Furthermore, calibration of the field magnitude is automatic if the ground state magnetic moment is known. Spectroscopy of the resolved sublevels gives us precise measurement of the differential *g*-factor, yielding 108.4(4) × m_F Hz/G [21, 1]. The resolved spectrum has also allowed experimental investigation of the tensor light shift sensitivity of the clock states,

demonstrating that they have a negligible impact on the current 1-D lattice clock [21].

3.3. *Hz-Resolution Optical Spectroscopy*

With the degeneracy of the clock states lifted in the presence of a magnetic field, the resolved transitions are explored free-of-broadening from the state-dependent

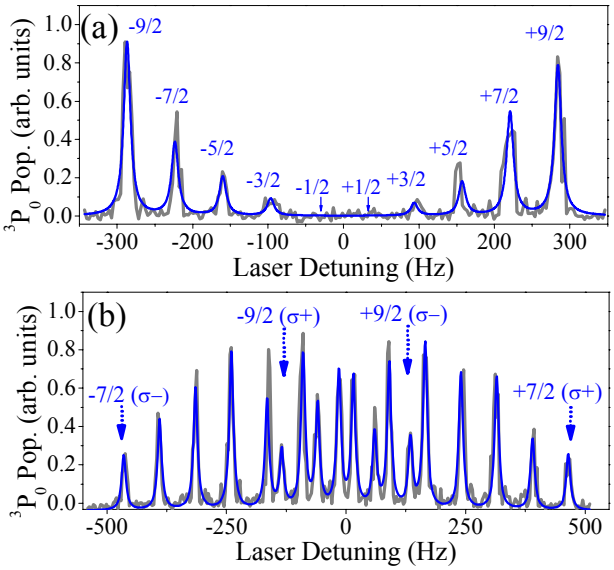

Figure 4. Spectroscopy of resolved m_F-sublevels in the presence of a magnetic bias field. (a) Ten π-transitions are observed when the probe is linearly polarized along the quantization axis set by a 0.58-G magnetic field. (b) When the probe polarization is orthogonal to the quantization axis, 18 σ transitions are seen, under a bias field of 0.69 G. In both (a) and (b), peaks are labeled according to the ground state m_F origin of the transition. In (b) the spectrum consists of two overlapped sets of nine evenly spaced peaks, the excitation polarization is labeled for clarity.

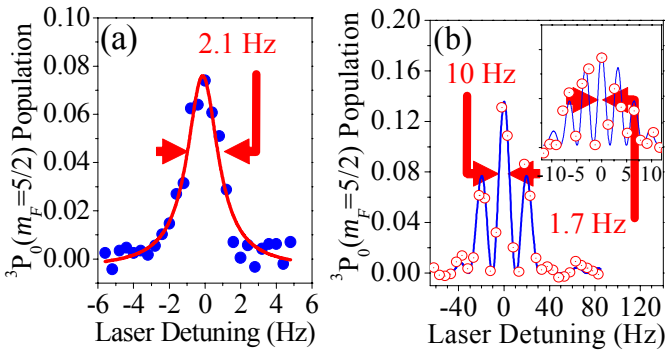

Figure 5. High-resolution spectroscopy of the clock transition for $m_F = 5/2$. (a) Ultra-narrow ($Q > 2 \times 10^{14}$) spectrum achieved with a 500-ms Rabi pulse. (b) Ramsey spectrum for 25-ms Ramsey pulses separated by a 80-ms evolution time, resulting in a 10 Hz FWHM for the central fringe. The inset shows the spectrum for longer pulse and free-evolution times of 80 ms and 200 ms, respectively. In both (a) and the inset of (b), the spectral resolution is limited by laser frequency noise during acquisition times of ~30 s.

Zeeman and Stark shifts, revealing the true spectroscopic limit of our system. An example spectrum is shown in Fig. 5(a), where the $^3P_0$ ($m_F = 5/2$) population is measured as the laser is tuned across the resonance. The resulting resonance width is 2.1(2) Hz ($Q > 2 \times 10^{14}$) [1], near the ~1.8 Hz Fourier limit set by the 500-ms interrogation time. Laser frequency noise prevents longer probe times as the beat between our two 698 nm lasers broadens to nearly 2 Hz when integrated over the relevant timescale for scanning the line (about 30 s). Ramsey spectroscopy can also be performed, as shown in Fig. 5(b). The Doppler-free absorption spectrum and long interaction time provided by the lattice confinement allows use of long, low-intensity pulses for the Ramsey sequence, resulting in simple spectra with a small number of fringes.

4. Clock Performance

The high-resolution spectroscopy results establish confidence in the lattice clock technique as a tool for precision measurement. The high stability oscillator, large line Q, and relatively large S/N can result in clock stability at the 1×10^{-15} level at 1 s. Another important issue is the level of accuracy that can be achieved with the lattice system.

4.1. *Accuracy Evaluation (2006): Degenerate Sublevels*

We first present an accuracy evaluation using degenerate sublevels without a bias magnetic field. To evaluate the accuracy of the ^{87}Sr lattice clock an

interleaved scheme is used where the parameters of interest are quickly varied during a scan of the transition, allowing extraction of the shift coefficient using the precision of the laser cavity as a reference. In this way, we explore a variety of systematic effects, with dominant contributions to the uncertainty budget being the lattice shift, density shift, and Zeeman shift. Operating at a lattice wavelength of 813.4280(5) nm, we find that the ac Stark shift for the typical trap depth is -2.5(6.0) $\times$ 10^{-16}. For the typical density of ~5 $\times$ 10^{11} cm^{-3}, the collision shift is constrained to be below 3.3 $\times$ 10^{-16}. Each of these effects is consistent with zero and limited by the statistical uncertainty associated with hundreds of measurements. The Zeeman sensitivity is found to be non-zero but < 5.3 $\times$ 10^{-16} when the residual magnetic field is controlled to 5 mG. Due to the differential *g*-factor, we zero and monitor the field to this level using the transition linewidth. The total uncertainty for lattice spectroscopy under these operating conditions is 9 $\times$ 10^{-16} [5].

As the spectroscopy systematic uncertainties are evaluated, an absolute frequency measurement is performed using the fiber link and a Cs-calibrated H-maser. After a 24 hour run, the frequency of the ^{87}Sr $^{1}S_0$-$^{3}P_0$ transition is determined to be 429,228,004,229,874.0 ± 1.1 Hz. The total uncertainty of 2.5 $\times$ 10^{-15} is dominated by the statistical uncertainty in the frequency comparison (1.4 $\times$ 10^{-15}) and the maser calibration (1.7 $\times$ 10^{-15}) [5]. Figure 6 summarizes the recent absolute frequency measurements made by the groups in JILA [4, 5], Paris [6, 22], and Tokyo [23]. The excellent agreement between independent groups speaks strongly for the ^{87}Sr lattice clock as a frequency standard.

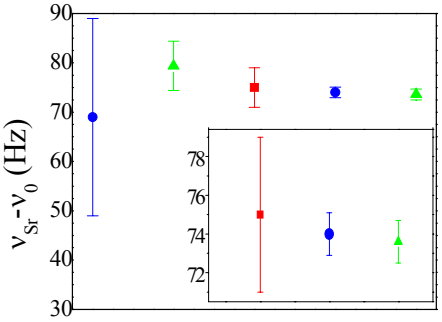

Figure 6. Recent absolute frequency measurements of the ^{87}Sr clock transition by JILA (circles), Paris (triangles), and Tokyo (squares). The frequency is reported relative to a set frequency ν_0 = 429,228,004,229,800 Hz. The inset shows a close-up view of the last three points on the main plot, with the last two [5, 21] differing by 7 $\times$ 10^{-16}.

4.2. *Accuracy Evaluation: Optical Clock Comparison with Spin-Polarized Samples*

Under its current operating parameters, the Sr lattice clock has a potential stability limit from quantum projection noise at 7×10^{-16} at 1 s. In practice, the stability is estimated to be 2×10^{-15} at 1 s, limited by the Dick effect of the optical local oscillator [24]. Such measurement stability cannot be fully exploited by comparison to current state-of-the-art microwave standards. Rather, accuracy evaluation of optical atomic clocks greatly benefits from direct comparison against other optical clocks with similar stability. Using the optical carrier transfer system described earlier, we now evaluate systematic uncertainties of the JILA Sr lattice clock by measurement against the cold Ca optical clock at NIST [15]. Figure 7 shows the measurement potential of a clock comparison between the ^{87}Sr lattice clock and the Ca clock. The stability at 1 s is $\sim 3 \times 10^{-15}$ and a precision of 3×10^{-16} is achieved in only 200 s of averaging. This frequency discrimination at relatively short averaging times facilitates high precision measurement of systematic shifts of the Sr clock. To reduce measurement sensitivity to long time-scale (>1000s) frequency drifts of the Ca standard, we measure frequency differences between sets of 100-s data under various Sr parameters to be evaluated. By collecting many sets of these data, we characterize systematic shifts below the 1×10^{-16} level.

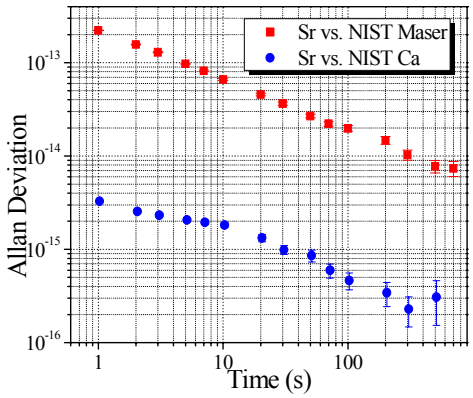

Figure 7. Microwave and optical clock comparisons using the fiber link discussed in the text. The Allan deviation for the Sr - Maser comparison is shown as squares, yielding a stability of $\sim 2.5 \times 10^{-13}\ \tau^{-1/2}$. The advantage of an optical clock is apparent from the Sr - Ca comparison (circles), which typically yields stability of 3×10^{-15} at 1 s.

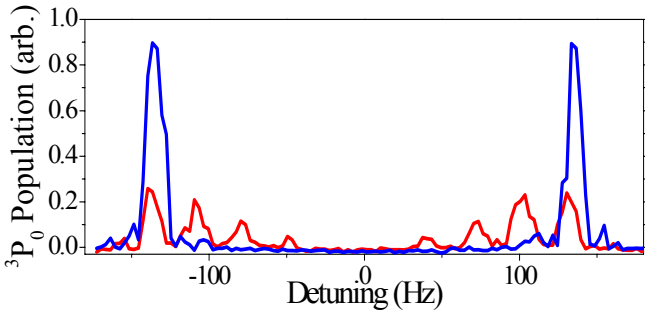

Figure 8. Spectroscopy of the π transitions under a bias magnetic field. Blue (dark gray) is with atomic polarization to $m_F = \pm 9/2$, and red (light gray) is without. The polarization is achieved by optical pumping using the $^1S_0$ F=9/2 - $^3P_1$ F=7/2 transition.

To reduce clock sensitivity to some key experimental parameters, we spin-polarize the Sr sample to the stretched nuclear spin states, $m_F = \pm 9/2$, and then perform spectroscopy with a small bias magnetic field to lift spin state degeneracy (see Fig. 8). By stabilizing the clock laser to the average of the π transitions from both spin states, we remove shifts originating from the 1st order Zeeman effect and the vector light shift due to the lattice confinement. The clock remains sensitive to 2nd order Zeeman shifts. As we vary the bias magnetic field and measure the clock frequency versus Ca, we confirm that the 1st order Zeeman effect is eliminated, resulting in a clock shift of $1.6(2.3) \times 10^{-17}$. Furthermore, we measure the 2nd order Zeeman shift at $5.8(0.8) \times 10^{-16}$ G^{-2}, resulting in a 2nd order frequency shift of $2.3(0.2) \times 10^{-17}$.

In addition to Zeeman shifts, we characterize systematic shifts resulting from: AC Stark effect from the lattice and probe lasers, atom servo error, blackbody AC Stark effect, atomic collisions, and higher order motional effects. A preliminary summary of these effects is given in Table 1. One of the largest observed shifts originates from density-dependent Sr-Sr interactions. Measurement of the clock shifts indicate that these interactions depend on both the nuclear spin state as well as the electronic excitation. We are currently investigating these effects in more detail and it is anticipated that a zero-density-shift condition will be found and implemented for the clock operation. The stated density shift and uncertainty in Table 1 are given for our current operating conditions. The total systematic shift uncertainty is $< 2 \times 10^{-16}$, indicating the strong performance of the Sr lattice clock as a potential primary frequency standard. We expect this uncertainty to continue to decrease.

Contributor	Correction	Uncertainty
Lattice Stark (scalar/tensor)	2.5	0.5
AC Stark (probe)	0.2	0.2
1^{st} order Zeeman	0.2	0.2
2^{nd} order Zeeman	0.2	0.02
Servo Error	0	0.5
Density	15	1
BBR Stark	52.1	1
Hyperpolarizability (lattice)	0	<0.2
Line Pulling	0	0.2
2^{nd} order Doppler	0	$\ll$0.01
Systematic total		1.7

Table 1. Systematic frequency corrections for the Sr lattice clock, and their respective uncertainties. All quantities are expressed in fractional frequency of 10^{-16}.

Conclusion

We have presented our recent results for an optical atomic clock based on strontium atoms confined in an optical lattice. The local oscillator is now performing at the 1×10^{-15} level at 1 – 1000 s, and the fiber/comb transfer system has been shown to support precision frequency transfer at the level of 1×10^{-17} at 1 s. The lattice clock technique, combined with the high precision laser, has yielded the highest line Q ($> 2 \times 10^{14}$) achieved in coherent spectroscopy, with a good S/N for further enhanced stability. Nuclear-spin effects in the lattice clock have been explored, including a measurement of the differential *g*-factor of the clock transition. An accuracy evaluation is performed, reducing the lattice clock systematics below 10^{-15}, and an absolute frequency measurement with a 1 Hz uncertainty is made, which is in excellent agreement with that of other groups. Comparison of the Sr clock with the NIST Ca clock revealed the clock instability is $< 3 \times 10^{-15}$ at 1 s. Using the high precision optical comparison and spin-polarized samples, the lattice clock systematic uncertainty has been reduced to 2×10^{-16} and it will continue to decrease in the near future.

Acknowledgments

We gratefully acknowledge contributions from J. Bergquist, T. Parker, S. Jefferts, and T. Heavner for help with the fiber-link-based laser comparison and the absolute frequency measurements made via the Sr - Maser comparison.

References

1. M. M. Boyd et al., “Optical atomic coherence at the 1-second time scale,” Science, vol. 314, pp. 1430-1433, 2006.

2. R. J. Rafac, B. C. Young, J. A. Beall, W. M. Itano, D. J. Wineland, and J. C. Bergquist, “Sub-dekahertz ultraviolet spectroscopy of 199Hg+,” Phys. Rev. Lett., vol. 85, p. 2462, 2000.
3. M. Takamoto, F.-L. Hong, R. Higashi, and H. Katori, “An optical lattice clock,” Nature, vol. 435, pp. 321-324, 2005.
4. A. D. Ludlow et al., “Systematic study of the 87Sr clock transition in an optical lattice,” Phys. Rev. Lett., vol. 96, p. 033003, 2006.
5. M. M. Boyd et al., “87Sr lattice clock with inaccuracy below 10-15,” Phys. Rev. Lett., vol. 98, p. 083002, 2007.
6. R. Le Targat et al., “Accurate optical lattice clock with 87Sr atoms,” Phys. Rev. Lett., vol. 97, p. 130801, 2006.
7. Z. W. Barber, C. W. Hoyt, C. W. Oates, L. Hollberg, A. V. Taichenachev, and V. I. Yudin, “Direct excitation of the forbidden clock transition in neutral 174Yb atoms confined to an optical lattice,” Phys. Rev. Lett., vol. 96, p. 083002, 2006.
8. A. D. Ludlow et al., “Compact, thermal-noise-limited optical cavity for diode laser stabilization at 1x10-15,” Opt. Lett., vol. 32, pp. 641-643, 2007.
9. M. Notcutt, L.-S. Ma, J. Ye, and J. L. Hall, “Simple and compact 1-Hz laser system via an improved mounting configuration of a reference cavity,” Opt. Lett., vol. 30, pp. 1815-1817, 2005.
10. K. Numata, A. Kemery, and J. Camp, “Thermal-noise limit in the frequency stabilization of lasers with rigid cavities,” Phys. Rev. Lett., vol. 93, p. 250602, 2004.
11. T. M. Fortier, D. J. Jones, and S. T. Cundiff, “Phase stabilization of an octave-spanning Ti:sapphire laser,” Opt. Lett., vol. 28, pp. 2198-2200, 2003.
12. T. P. Heavner, S. R. Jefferts, E. A. Donley, J. H. Shirley, and T. E. Parker, “NIST-F1: recent improvements and accuracy evaluations,” Metrologia, vol. 42, p. 411, 2005.
13. J. Ye et al., “Delivery of high-stability optical and microwave frequency standards over an optical fiber network,” JOSA B, vol. 20, pp. 1459-1467, 2003.
14. S. M. Foreman, K. W. Holman, D. D. Hudson, D. J. Jones, and J. Ye, “Remote transfer of ultrastable frequency references via fiber networks,” Rev. Sci. Instrum., vol. 78, p. 021101, 2007.
15. C. W. Oates, E. A. Curtis, and L. Hollberg, “Improved short-term stability of optical frequency standards: approaching 1 Hz in 1 s with the Ca standard at 657 nm,” Opt. Lett., vol. 25, pp. 1603-1605, 2000.
16. W. H. Oskay et al., “Single atom optical clock with high accuracy,” Phys. Rev. Lett., vol. 97, p. 020801, 2006.
17. T. M. Fortier, A. Bartels, and S. A. Diddams, “Octave-spanning Ti:Sapphire laser with a repetition rate > 1 GHz for optical frequency measurements and comparisons,” Opt. Lett., vol. 31, pp. 1011-1013, 2006.

18. S. M. Foreman et al., "Coherent optical phase transfer over a 32-km fiber with long-term instability $<10^{-18}$," Phys. Rev. Lett., in press, 2007.
19. B. C. Young, F. C. Cruz, W. M. Itano, and J. C. Bergquist, "Visible lasers with subhertz linewidths," Phys. Rev. Lett., vol. 82, p. 3799, 1999.
20. T. Loftus, T. Ido, A. D. Ludlow, M. M. Boyd, and J. Ye, "Narrow line cooling: finite photon recoil dynamics," Phys. Rev. Lett., vol. 93, p. 073003, 2004; T. Loftus, T. Ido, M. M. Boyd, A. D. Ludlow, and J. Ye, "Narrow line cooling and momentum-space crystals," Phys. Rev. A, vol. 70, p. 063413, 2004.
21. M. M. Boyd et al., "Nuclear spin effects in optical lattice clocks," Phys. Rev. A, vol. 76, p. 022510, 2007.
22. P. Lemonde et al., "An optical lattice clock with spin-polarized 87Sr atoms," Proceedings of the Joint 2007 European Frequency and Time Forum & 2007 IEEE Frequency Control Symposium, Geneva, Switzerland, May 28th-June 1st, 2007.
23. M. Takamoto, F.-L. Hong, R. Higashi, Y. Fujii, M. Imae, and H. Katori, "Improved frequency measurement of a one-dimensional optical lattice clock with a spin-polarizaed fermionic 87Sr isotope," J. Phys. Soc. Japan, vol. 75, p. 104302, 2006.
24. G. Santarelli, C. Audoin, A. Makdissi, P. Laurent, G. J. Dick, and A. Clairon, "Frequency Stability Degradation of an Oscillator Slaved to a Periodically Interrogated Atomic Resonator," IEEE Trans. On Ultrasonics, Ferroelectrics, and Frequency Control, vol. 45, no. 4, July 1998.